Experimental investigation of absorption in upward and downward flow of NH_3-CO_2-H_2O in a mini-channel heat exchanger

Shi, Liang; Gudjonsdottir, V.; Infante Ferreira, C. A.

DOI
10.1016/j.ijheatmasstransfer.2020.119483

Publication date
2020

Document Version
Final published version

Published in
International Journal of Heat and Mass Transfer

International Journal of Heat and Mass Transfer 152 (2020) 119483

Contents lists available at ScienceDirect

International Journal of Heat and Mass Transfer

journal homepage: www.elsevier.com/locate/hmt

Experimental investigation of absorption in upward and downward flow of NH_3-CO_2-H_2O in a mini-channel heat exchanger

V. Gudjonsdottir*, L. Shi, C.A. Infante Ferreira

Process and Energy Laboratory, Delft University of Technology, Leeghwaterstraat 39, 2628 CB, Delft, The Netherlands

ARTICLE INFO

Article history:
Received 11 September 2019
Revised 22 January 2020
Accepted 5 February 2020

Keywords:
Heat pumps NH_3-CO_2-H_2O NH_3-H_2O absorption mini-channel heat exchanger

ABSTRACT

Heat pumps can drastically reduce energy requirements in industry. Operating a compression resorption heat pump with an NH_3-CO_2-H_2O mixture has been identified as a promising option that can have an increased performance compared to only NH_3-H_2O. In this paper an important process of the heat pump cycle is investigated: The absorption process. A mini-channel heat exchanger with 116 tubes of inside diameter of 0.5 mm is used for this purpose. For the NH_3-H_2O experiments overall heat transfer coefficients of 2.7–6 kW/(m^2K) were reached for mixture mass flows of 0.71–2.5 kg/h. For the NH_3-CO_2-H_2O mixture pumping instabilities limited the operating range which resulted in higher pressures and higher mixture mass flows compared to NH_3-H_2O. The overall heat transfer coefficients were lower in the case of the added CO_2, with the maximum of 3 kW/(m^2K) corresponding to a mixture mass flow of 4.2 kg/h. However, an increase in heat transfer of approximately 5% was reached with the added CO_2 which is beneficial for heat pump applications. Additionally, limited research has been conducted on absorption in upward versus downward flow and, therefore, these two configurations have also been tested in the mini-channel heat exchanger. Even though the pumping instabilities vanished with absorption in upward flow it was confirmed that absorption in downward flow with the mixture on the tube side is the most beneficial configuration for absorption of ammonia in NH_3-CO_2-H_2O or NH_3-H_2O in a mini-channel heat exchanger. The performance increased by approximately 10% with absorption in downward flow.

1. Introduction

Drastic measures are necessary if the goal of the Paris agreement is to be realized, to keep the temperature rise under 2 °C during this century [1]. Industrial processes need to become more sustainable. Heat pumps are one of the solutions that can drastically reduce energy consumption in industry. One of the main problems is long payback periods [2]. Compression-resorption heat pumps (CRHPs) have the potential to have better performance compared to traditional technologies. Utilizing alternative working fluids, said potential can be even further increased. NH_3-CO_2-H_2O has been identified as a promising alternative [3]. The study reported in [3] showed, with simulations, that the heat pump performance could be increased by approximately 5% with the NH_3-CO_2-H_2O mixture compared to only NH_3-H_2O. CRHPs have four main components, a resorber, desorber, a compressor and an expansion valve. In the resorber absorption of NH_3 in NH_3-H_2O or NH_3-CO_2-H_2 takes place. This process can be improved by using compact heat exchangers instead of traditional ones [4].

Compact heat exchangers can decrease energy requirements and costs compared to traditonal heat exchangers [4]. Mini/micro-channels can have even better heat transfer performance, and be even more compact than conventional compact heat exchangers like plain-fins, wavy fins and fin-tubes [4,5]. A comprehensive review is given by Khan and Fartaj [5] on microchannel heat exchangers, defined to have channels $\leq$ 1 mm. As these authors mention the potentials are great, however, more research is necessary. There is especially limited research related to large scale thermal and energy applications of micro-channel heat exchangers [5].

For NH_3-H_2O absorption the most common methods of operation are bubble or falling film absorption [6]. A comprehensive review is given by Amaris et al. [6]. These authors mention that the falling film absorption has been more commonly applied and

Abbreviations: CHX, Coiled heat exchangers; CRHPs, Compression-resorption heat pumps; e-NRTL, Electrolyte - Non-Random Two-Liquid; LMTD, Logarithmic mean temperature difference; MCGP, Magnetically coupled gear pumps; PHX, Plate heat exchangers.

* Corresponding author.
E-mail address: v.gudjonsdottir@tudelft.nl (V. Gudjonsdottir).

https://doi.org/10.1016/j.ijheatmasstransfer.2020.119483

Nomenclature

A	Area m^2
Bi	Biot number: $Bi = \frac{hc_s r_t}{\lambda}$
c_p	Isobaric heat capacity J kg^{-1} K^{-1}
d	Tube diameter m
Gz	Graetz number: $Gz = \frac{\dot{m}_s c_p}{N\lambda_s z}$
h	Specific enthalpy J kg^{-1}
hc	Heat transfer coefficient W m^{-2} K^{-1}
L	Heat exchanger length m
$\dot{m}$	Mass flow kg s^{-1}
N	Number of tubes
N_m	Number of measurements
Nu	Nusselt number: $Nu = \frac{hc\, d_H}{\lambda}$
P	Pressure Pa
p	Tube pitch m
$\dot{Q}$	Heat duty W
r	Radius m
T	Temperature K
U	Overall heat transfer coefficient W m^{-2} K^{-1}
u	Uncertainty
x	Mass concentration kg kg^{-1}
z	Axial position in the heat exchanger m

Greek symbols

α	Dimensionless spacing between tubes
β	Pitch-to-tube diameter ratio
Δ	Difference
λ	Thermal conductivity W m^{-1} K^{-1}
σ	Standard deviation

Subscripts

calc	Calculated
f	Derived variable
H	Hydraulic
in	Inlet
lm	Logarithmic mean
out	Outlet
s	Shell side
t	Tube side
x, z	Measured variables

that it is the preferred operating option for many researchers [7,8]. As mentioned by Trichè et al. [7] the performance varies greatly depending on the absorption operating method and the specific geometry. According to their prediction the falling film mode is the preferred one. It is clear that very limited studies in the open literature compare directly the two absorption modes, especially experimentally. Kang et al. [9] investigated analytically the two different absorption operating modes and concluded that the local absorption rate was always higher for the bubble mode. Castro et al. [10] investigated experimentally the two modes for air-cooled absorption systems. The bubble absorption was generally more efficient, especially for low solution flow rates because of the low wetted area of the falling film. As mentioned by van Leeuwen [11] the flow patterns in mini-channel heat exchangers are significantly different from in traditional absorbers. Therefore, falling film and bubble absorption might not be descriptive for those kind of heat exchangers. More accurate is to talk about absorption in upward or downward flow.

When it comes to absorption of NH_3-H_2O in micro- or mini-channel heat exchangers several studies have been conducted. Garimella et al. [12] studied the absorption process in a microchannel heat exchanger. They improved an existing design and reached overall heat transfer coefficients in the range of 0.54–1.16 kW/(m^2K). In mini-channels the absorption process of NH_3-H_2O has previously been studied by Van Leeuwen [11] and van de Bor et al. [13]. Van Leeuwen [11] performed experiments with single tube mini-channel heat exchanger using tube diameters of about 1.1 and 2.0 mm. His conclusion was that the overall heat transfer coefficient increased with decreased diameter and that the overall heat transfer coefficient was significantly higher than for conventional heat exchangers. This is similar to the findings of Amaris et al. [14] for tubular bubble absorbers and Yoon et al. [15] for falling film absorbers. According to the VDI Heat Atlas [16] conventional heat exchangers, like shell and tube and plate heat exchangers, have an overall heat transfer coefficient in the range from 1 to 4 kW/(m^2K). Van Leeuwen [11] reached values from approximately 6 to 13 kW/(m^2K) for a tube diameter of 1.1 mm and predicted values up to 25 kW/(m^2K) for 0.5 mm tubes.

As was mentioned before, there is a need to scale up micro- and minichannel heat exchangers [5]. The heat exchanger used in this paper is a multi-tube (116 tubes) mini-channel heat exchanger with an inside diameter of 0.5 mm. This heat exchanger was designed as a first step in scaling up mini-channel heat exchangers. Experimental results with the current heat exchanger have previously been reported for water-water experiments [17] and with NH_3-H_2O [18]. The heat transfer performance was, unfortunately, lower than expected with the highest overall heat transfer coefficients only around 2 kW/(m^2K). It was concluded that the decrease in performance was due to hydrodynamic instabilities. In the study by van de Bor [18] the NH_3-H_2O mixture was either on the shell side or both on shell and tube side of the heat exchanger. These results were still considerably higher than reported by Lee at al [19]. where NH_3-H_2O bubble absorption was performed in a plate heat exchanger with a maximum overall heat transfer coefficient of around 0.6 kW/(m^2K). The results from van de Bor [18] were also slightly higher than the results reported by Lee et al. [20] for horizontal tube falling-film flow where the overall heat transfer coefficient ranged from 0.7-1.9 kW/(m^2K). Various other researches for either bubble absorption or falling film flow with NH_3-H_2O have been reported for plate heat exchangers [7,21,22]. In these cases the heat transfer performance was also worse than for the mini-channel reported by van de Bor [18]. In all the cases mentioned above the temperature difference was calculated with the logarithmic mean temperature difference (LMTD), except in the case of van de Bor [18] and Trichè et al. [7] where the absorber was divided into control volumes and the average of the calculated local temperature difference was used. Even though the mini-channel heat exchanger could be further optimized, it is well suitable for comparing the absorption process of NH_3-H_2O and of NH_3-CO_2-H_2O mixtures.

In this study first water-water experiments are performed with the current mini-channel heat exchanger, then the water on the tube side is replaced by NH_3-H_2O and, finally, CO_2 is added to the NH_3-H_2O mixture. The water-water experiments are compared with existing prediction methods for both sides of similar heat exchanger arrangements. In the NH_3-H_2O experiments as well as in the initial NH_3-CO_2-H_2O experiments absorption in downward flow takes place. The last set of experiments investigate the effects when the absorption process takes place in upward flow.

2. Experimental setup

The design of the mini-channel heat exchanger is illustrated in Figs. 1 and 2. The heat exchanger was designed as a first step in scaling up mini-channel heat exchangers for industrial use [18]. The heat exchanger is oven-brazed and the length of the heat exchanger was limited by the physical dimensions of the brazing

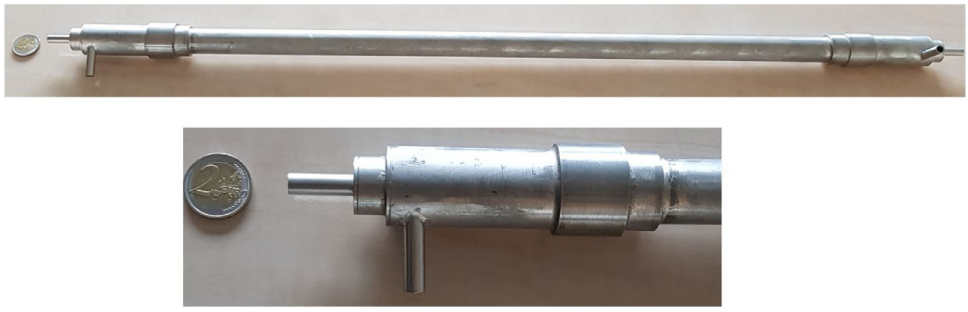

Fig. 1. Photographs of the investigated mini-channel heat exchanger. The 2 € coin clarifies the dimension of the heat exchanger. For detailed dimensions see Table 1.

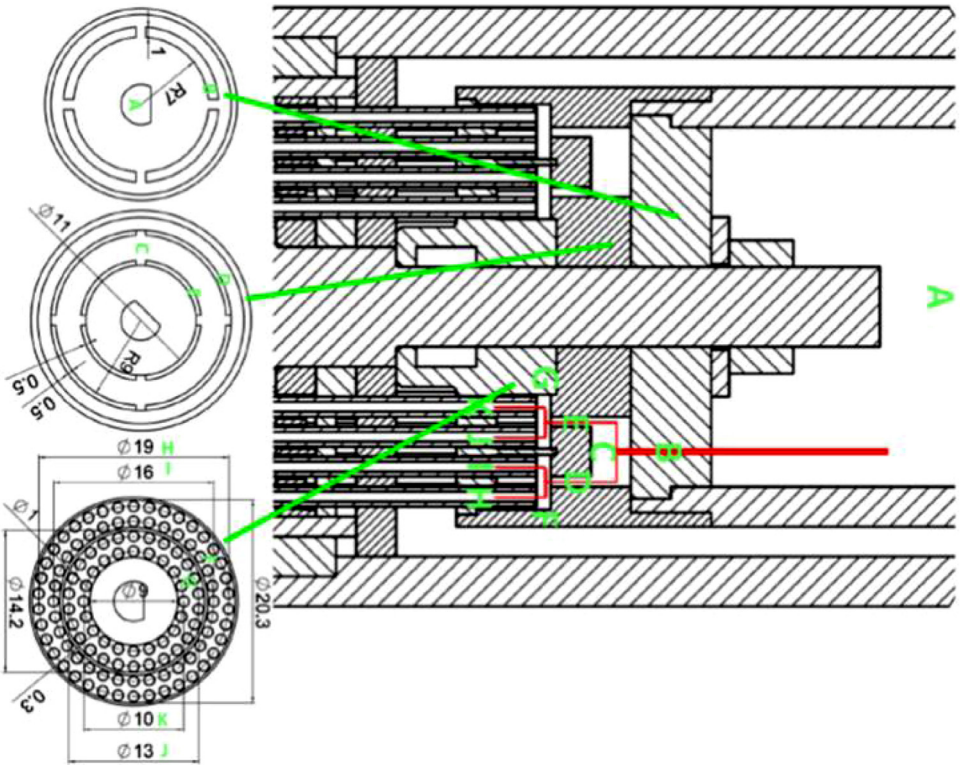

Fig. 2. Illustration of the fractal distribution that is used both on tube and shell sides of the mini-channel heat exchanger to guarantee pure countercurrent flow of the heat exchanger fluids [17]. The bottom left figure shows how the tubes are arranged in the shell of the heat exchanger.

Table 1
The mini-channel heat exchanger main geometrical characteristics. Additonal details can be found in the study by Nefs et al. [17].

Number of tubes	116
Heat exchanging length, mm	652
Total length of heat exchanger, mm	800
Inner tube diameter, mm	0.5
Outer tube diameter, mm	1.0
Inner shell diameter, mm	21
Outer shell diameter, mm	25
Shell hydraulic diameter, mm	1.8
Tube pitch, mm	0.78
Tube side heat exchanging area, m^2	0.146

oven, resulting in total heat exchanger length of 0.8 m [23]. This size was still considered a good first step before further scale up. The tube diameter and number of tubes were the results of an optimization study done by Ozgur [23]. He investigated which size would lead to acceptable pressure drops, resulting in an inner diameter of 0.5 mm and 116 tubes. To guarantee pure counter current flow, fractal distribution is used on both tube and shell sides. The main geometrical characteristics of the heat exchanger are listed in Table 1. The reader is referred to Nefs et al. [17] for additional details regarding the design of the heat exchanger.

2.1. Description of the set-up

A simplified process and instrumentation diagram of the experimental setup is shown in Fig. 3. The setup consists of two almost identical loops. One for the shell side of the mini-channels and the other for the tube side. In each loop the flow is driven by magnetically coupled gear pumps (MCGP) that are coupled to a Coriolis flow meter that, additionally to the flow, provides density and temperature measurements. To reach the desired conditions at the inlet of the heat exchanger the flow circulates through coiled heat exchangers (CHX), in which hot oil from a thermostatic bath circulates through the annulus side. There is a slight temperature fluctuation in the oil bath. Therefore, to reach a better accuracy, the flow is additionally heated, by an electric tracing, to the desired conditions. After exiting the mini-channel heat exchanger, the fluid is cooled by the means of cooling water in a plate heat exchanger (PHX) to subcooled conditions. This is to prevent cavi-

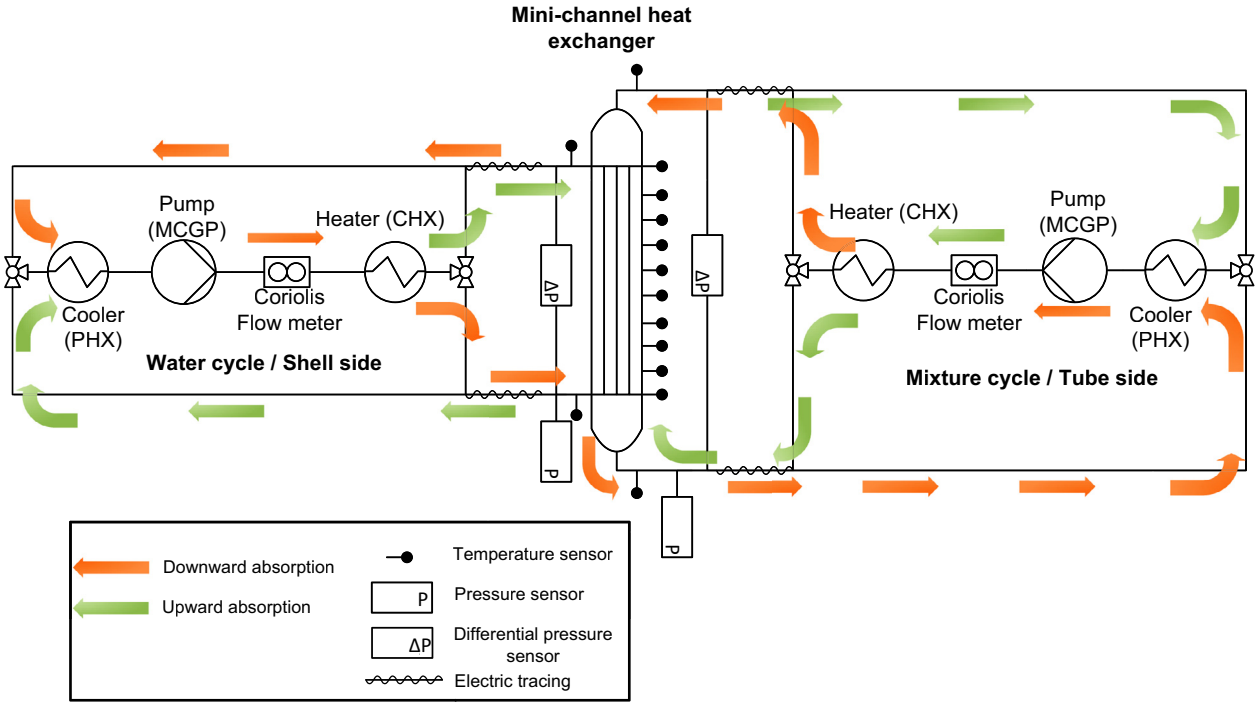

Fig. 3. A simplified process and instrumentation diagram of the mini-channel test setup. It is possible to operate the setup with absorption in downward flow (indicated with orange arrows) or in upward flow (indicated with green arrows). (For interpretation of the references to colour in this figure legend, the reader is referred to the web version of this article.)

Table 2
Type, range and accuracy of the sensors used in the mini-channel heat exchanger experiments.

Sensor type	Range	Accuracy	Unit
PT-100, Type B, temperature sensors	-50... +200	± 0.05	°C
Bronkhorst Mini Cori-Flow, M14, mass flow sensors	0... +20	± 0.04	kg/h
Bronkhorst Mini Cori-Flow, M14, density sensors	n. a.	± 5	kg/m^3
Bronkhorst Mini Cori-Flow, M14, temperature sensors	0.+70	± 0.5	°C
Siemens Sitrans P DS III, 7MF4033, pressure sensors	-1... +15	± 0.13	barg
Siemens Sitrans P DS III, 7MF4333, differential pressure sensors	-1600... +1600	± 8	mbarg

tation in the pumps. Temperature sensors are located both at the in- and outlet of both the tube and shell sides of the mini-channel heat exchanger. Pressure and differential pressure sensors are also located at the in- and outlet to provide the pressure drop over the tube and shell sides. The specifications and accuracy of all the sensors are listed in Table 2. Additionally, there are ten temperature sensors located along the shell of the mini-channel heat exchanger. These have rather low accuracy, around ± 1 ◦C. They still give a good idea of the temperature profile along the heat exchanger. As shown in Fig. 3, the set-up is configured in such a way that absorption in both downward and upward flow is possible. Fig. 4 shows three photographs of the set-up where the locations of the main components are highlighted. The water/shell sides are located in one fume hood and the mini-channel heat exchanger in another one next to it. The photograph of the mini-channel shows how the temperature sensors are located along the shell of the heat exchanger.

2.2. Heat transfer calculations and error propagation

The heat duty of the tube and shell sides are calculated with the following equation [24]:

$$\dot{Q} = \dot{m}(h_{out} - h_{in}) \tag{1}$$

where the enthalpy for the water and NH_3-H_2O are determined with the Refprop database [25] and the new fit from Gudjonsdottir et al. [3] is used for the NH_3-CO_2-H_2O mixture. The overall heat transfer coefficient is determined as:

$$U = \frac{\dot{Q}}{A\Delta T_{lm}} \tag{2}$$

where the heat flow is the uncertainty-weighted average of the shell and tube side as described by Park et al. [26]

$$\bar{\dot{Q}} = \phi_t \dot{Q}_t + \phi_s \dot{Q}_s \tag{3}$$

where ϕ_t and ϕ_s are weight factors dependent on the uncertainty of each heat flow, they are described further in this section along with the uncertainty. The contact area is estimated as:

$$A = \pi d N L \tag{4}$$

where, d, is the internal tube diameter, N, the number of tubes and, L, is the length of the heat exchanger. The LMTD is calculated as:

$$\Delta T_{lm} = \frac{(T_{t,in} - T_{s,out}) - (T_{t,out} - T_{s,in})}{ln\left(\frac{T_{t,in} - T_{s,out}}{T_{t,out} - T_{s,in}}\right)} \tag{5}$$

It should be noted that in the case of NH_3-H_2O and NH_3-CO_2-H_2O mixture the thermal properties vary considerably within the mini-

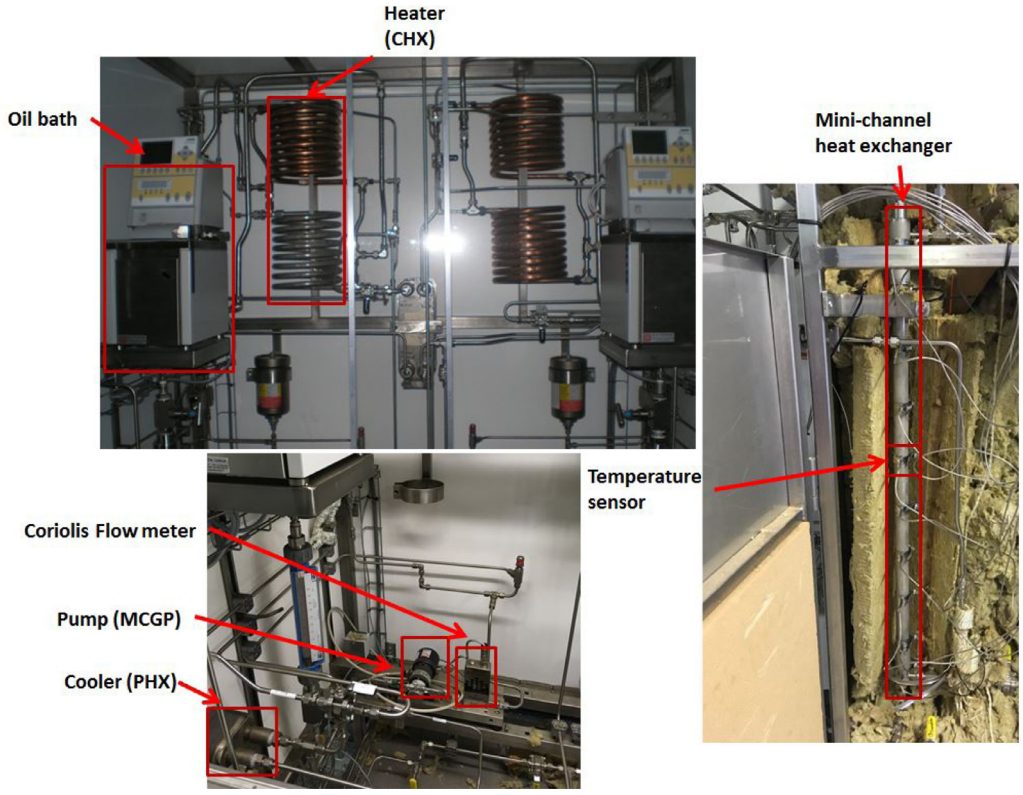

Fig. 4. Photographs of the experimental set-up. The two photographs on the left are from a cabinet containing the water and mixture cycles. The photograph on the right is from a separate fume hood where the mini-channel heat exhanger is located.

channel heat exchanger and, therefore, the actual average temperature difference can differ from the estimated LMTD. The LMTD and overall heat transfer coefficient results should in those cases be taken with caution. For error propagation the method described by Taylor [27] is used. The general formula for determining the uncertainty of a function, f, can be described as:

$$u_f = \sqrt{\left(\frac{\delta f}{\delta x}u_x\right)^2 + \ldots + \left(\frac{\delta f}{\delta z}u_z\right)^2} \tag{6}$$

where $x, \ldots, z$ are measured variables with uncertainties $u_x, \ldots, u_z$. If the relationship of the function is unknown then the uncertainty can be calculated as:

$$u_f = \sqrt{(f(x+u_x, \ldots, z) - f(x, \ldots, z))^2 + \ldots + (f(x, \ldots, z+u_z) - f(x, \ldots, z))^2} \tag{7}$$

The uncertainty of each heat flow is, therefore, calculated as follows:

$$u_{\dot{Q}} = \sqrt{\left(\frac{\delta \dot{Q}}{\delta \dot{m}}u_{\dot{m}}\right)^2 + \left(\frac{\delta \dot{Q}}{\delta h_{out}}u_{h_{out}}\right)^2 + \left(\frac{\delta \dot{Q}}{\delta h_{in}}u_{h_{in}}\right)^2} \tag{8}$$

where the uncertainty of the enthalpy is determined as:

$$u_h = \left((h(T+u_T, P, x) - h(T, P, x))^2 + (h(T, P+u_p, x) - \ldots \right. \\ \left. h(T, P, x))^2 + (h(T, P, x+u_x) - h(T, P, x))^2\right)^{1/2} \tag{9}$$

The weight factors for the uncertainty-weighted average can then be determined as [26]:

$$\phi_t = \frac{u_{\dot{Q}_s}^2}{u_{\dot{Q}_s}^2 + u_{\dot{Q}_t}^2} \tag{10}$$

$$\phi_s = \frac{u_{\dot{Q}_t}^2}{u_{\dot{Q}_s}^2 + u_{\dot{Q}_t}^2} \tag{11}$$

And the uncertainty of the weighted average [28]

$$u_{\bar{\dot{Q}}} = \sqrt{\phi_t^2 u_{\dot{Q}_t}^2 + \phi_s^2 u_{\dot{Q}_s}^2} \tag{12}$$

The uncertainty of the LMTD and the overall heat transfer coefficient are estimated in a similar way. Additionally, to account for fluctuations during the experiments the standard deviation of the mean is used

$$u_x = \sigma_{\bar{x}} = \sigma_x / \sqrt{N_m} \tag{13}$$

It should be noted that in most cases discussed in this paper this is negligible compared to the accuracy of the sensors.

3. Experimental results and analysis

The following sections display the experimental results. The uncertainty and error bars are included where applicable, except where they would be barely visible. Firstly, experiments were performed with water on both the shell and tube side. Thereafter, with NH_3-H_2O mixture on the tube side of the heat exchanger and, lastly, with NH_3-CO_2-H_2O mixture on the tube side.

3.1. Water-water experiments

Initially, experiments with water on both the shell and tube side were performed. The water entered at the top of the tube side and at the bottom of the shell side. The operating conditions are listed in Table 3. The large temperature glides of the flows correspond to the expected operating conditions in industrial heat pump applications. The operating pressure was around $8 \cdot 10^5$ Pa for the shell side during the experiments and around $6 \cdot 10^5$ Pa at the tube side.

With these experiments it could be determined if sufficient insulation around the mini-channel heat exchanger was used.

Table 3
Conditions to be tested during water-water experiments.

Tube side mass flow, $\dot{m}_s$	10 kg/h
Shell side mass flow, $\dot{m}_t$	2.5 - 20 kg/h
Shell side inlet temperature, $T_{s,in}$	60 °C
Tube side inlet temperature, $T_{t,in}$	110 °C

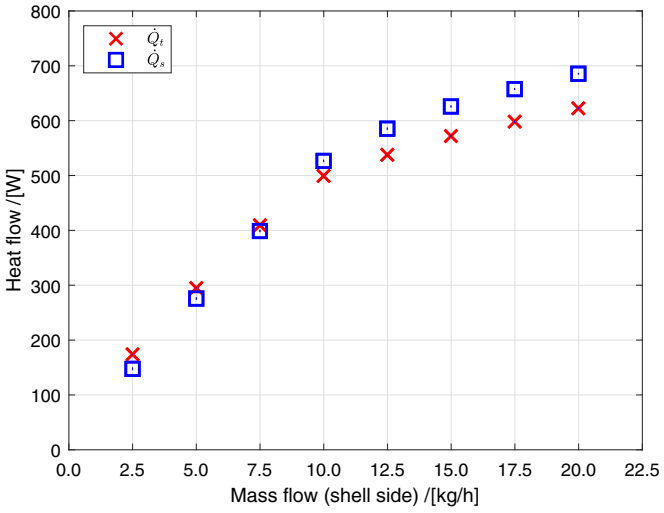

Fig. 5. Heat flow of the shell side, $\dot{Q}_s$, and tube side, $\dot{Q}_t$, for the water-water experiments.

Initially, additional insulation was added until the difference in the heat flow of the tube and shell side was within 5% for a mass flow of 10 kg/h. Then other shell side mass flows were tested. Fig. 5 shows the comparison of the heat flows. In all cases the difference is less than 10%. It is expected that the shell side heat flow is slightly lower than the tube side since the insulation can not completely hinder some losses to the environment. This is seen for the lower shell side mass flows. At the higher mass flows an opposite trend is seen. The uncertainty of the measurements is very low in these cases, only around $\pm$ 2 W, while the difference in the most extreme case, at 20 kg/h, is 63 W. Fig. 6 illustrates how the shell side flow is collected and flows through an annulus space along the tube side inlet flow before leaving the heat exchanger. The temperature difference between the two flows in this region may explain the additional temperature rise of the shell side flow which is detected by the outlet temperature sensor just after the heat exchanger.

For the water-water experiments the method provided by Nefs et al. [17] for the prediction of the heat transfer performance of the heat exchanger has been applied. There the heat transfer coefficient is a function of the Nusselt number:

$$hc = Nu\frac{\lambda}{d_H} \tag{14}$$

The tube side heat transfer coefficient is then calculated with the method proposed by Sparrow and Patankar [29] for laminar single phase flow in tubes (defined for Reynolds Numbers lower than 2300). In their case the Nusselt number is related to the Biot number of the flow. The Biot number is defined as:

$$Bi = hc_s * r_t/\lambda \tag{15}$$

The Nusselt number is then defined in the following way:

$$\begin{array}{ll} Nu = 4.364 & Bi = 0 \\ Nu = 4.330 & 0 < Bi \leq 0.1 \\ Nu = 4.284 & 0.1 < Bi \leq 0.25 \\ Nu = 4.221 - (Bi - 0.5)(4.221 - 4.112)/0.5 & 0.25 < Bi \leq 0.5 \\ Nu = 4.122 - (Bi - 1)(3.997 - 4.122)/0.5 & 0.5 < Bi \leq 1 \\ Nu = 3.997 & 1 < Bi \leq 2 \\ Nu = 3.840 & 2 < Bi \leq 5 \\ Nu = 3.758 & 5 < Bi \leq 10 \\ Nu = 3.663 & 10 < Bi \leq 100 \\ Nu = 3.657 & Bi > 100 \end{array} \tag{16}$$

The shell side Nusselt number is calculated by the method provided by Miyatake and Iwashita [30] for a single phase thermally developed laminar flow along a tube bundle.

$$Nu = (c^2 + e^2 \cdot Gz^{2/3})^{1/2} \tag{17}$$

where

$$c = \frac{3.1\alpha^{0.1} + 324\alpha^{16}}{1 + 69.5\alpha^{24}} \tag{18}$$

$$e = \frac{1.536(1 + 8.24\alpha^{0.39})}{(2\sqrt{3}\beta - \pi)^{1/3}(1 + 6.37\alpha^{0.73})} \tag{19}$$

where the local Graetz number, pitch-to-tube diameter ratio and dimensionless spacing between tubes are defined as:

$$Gz = \frac{\dot{m}_s c_p}{N\lambda_s z} \tag{20}$$

$$\beta = \frac{2p}{d_{out,t}} \tag{21}$$

$$\alpha = \beta - 1 \tag{22}$$

In all tested cases the flow was laminar with a local Graetz number of less than 500. Therefore, it can be concluded that the shell side flow was indeed thermally developed laminar flow and the method provided by Miyatake and Iwashita [30] should give sufficiently accurate results. Fig. 7 shows the inlet and outlet temperatures of the different experiments, both the experimental

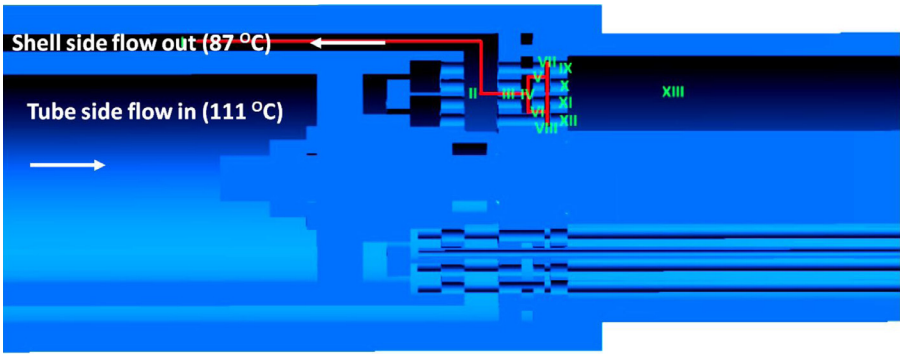

Fig. 6. Illustration of the shell side outlet of the mini-channel heat exchanger. The temperatures correspond to the measured temperature values of the water-water experiments when the shell side mass flow is kept at 20 kg/h.

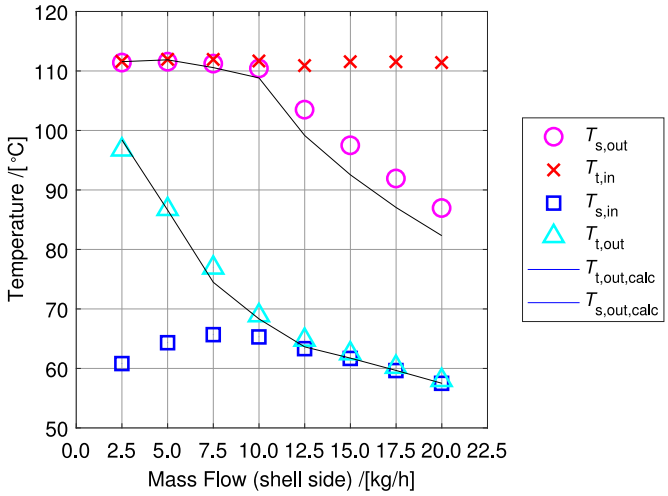

Fig. 7. In- and outlet temperatures for the water-water experiments. The tube side mass flow is kept constant at 10 kg/h while the shell side mass flow ranges from 2.5 to 20 kg/h. The markers are the experimental values while the solid lines are calculated with the method proposed by Nefs et al. [17] and discussed above.

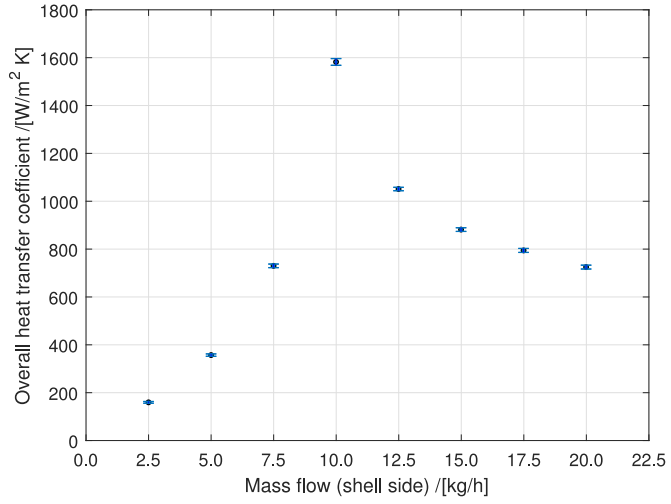

Fig. 8. Experimental overall heat transfer coefficient based on the tube side area for the water-water experiments. Error bars are included (see Section 2.2 for details).

values and the outlet values calculated with the method proposed by Nefs et al. [17]. The calculated values correspond quite well with the measured values. Since the same working fluid is on both sides of the heat exchanger it is not surprising that the ideal shell side mass flow is 10 kg/h, or when it is identical to the tube side mass flow. At these conditions the temperature differences between the shell and tube sides are minimal and the overall heat transfer coefficient is maximized (see Figs. 7 and 8). The error for the overall heat transfer coefficient ranges from $\pm$ 4 to 14 $Wm^{-2}K^{-1}$ in this case. For different working fluids, the mass flow ratio that gives the optimal results will vary. In the following section a similar procedure will be carried out to attempt to find the optimum mass flow for the different working fluids.

In Fig. 7 the method proposed by Nefs et al. [17], which has been introduced above, has been used to predict the outlet conditions of the tube and shell sides using the inlet conditions as inputs. The calculated values are represented by solid lines while the markers represent the experimental values. It is seen from the figure that the method comes very close to predict the outlet conditions of the experiments. Fig. 9 shows the results of the prediction method (solid lines) compared to the sensors values along the

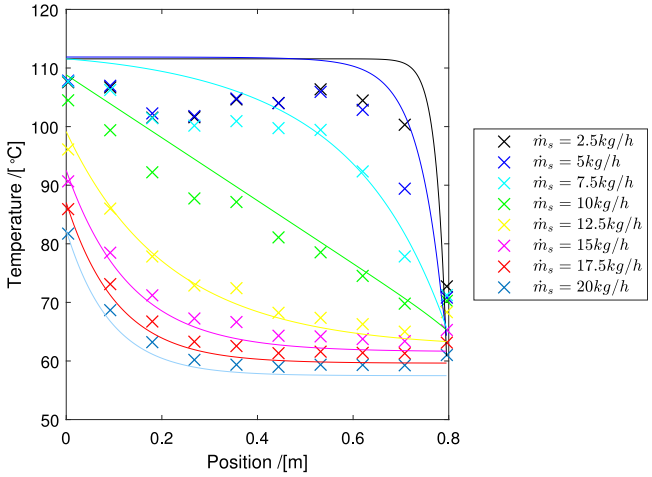

Fig. 9. Temperatures along the length of the heat exchanger for the water-water experiments. Solid lines are calculated temperatures of the shell side flow with the method proposed by Nefs et al. [17], that is described above, and the marker values are from the temperature sensors along the heat exchanger.

shell (marker values). It is seen that the profiles are very well represented except at the higher temperature where the sensor values are lower than the predicted profiles, although the trend is still the same. Since these temperature sensors are located at the outside of the heat exchanger it is likely that the insulation was insufficient for the sensors to represent accurate values at these temperatures.

3.2. NH_3-H_2O experiments

After the water-water experiments the tube side was filled with an NH_3-H_2O mixture, 33.5 wt% NH_3. This concentration was chosen since at atmospheric conditions the pressure is around $1 \cdot 10^5$ Pa. The theoretical optimum for CRHPs is achieved when the mixture enters the absorber as saturated vapor and leaves as saturated liquid [31]. Reaching these exact conditions in the set-up proved to be quite difficult and if the mixture at the in- or outlet of the heat exchanger was in the two phase region the temperature and pressure measurements were quite unstable. Therefore, it was imposed that the mixture enters slightly superheated and leaves slightly subcooled. To match these conditions the tube side inlet temperature was set around 130 °C and the shell side inlet temperature around 50 °C. The operating conditions are listed in Table 4.

For each shell side mass flow an attempt was made to find the optimum tube side mass flow with the procedure described in the previous section. As an example, the results for a shell side mass flow of 7.5 kg/h are shown in Figs. 10 and 11. The optimum tube side mass flow in this case was around 1.05 kg/h. For this condition the superheated and subcooled regions (flatter trend in Fig. 10) are minimized as well as the temperature difference between the shell and tube sides. From Fig. 10 it is also clear that the absorption of NH_3 takes up only a small portion of the heat exchanger. The mass flows were limited by the limits of the pumps, however, this indicates that the heat exchanger is oversized for these flows. Fig. 11 shows that the target temperature difference between in- and outlet of both sides of the heat exchanger is smallest when

Table 4
Conditions to be tested during NH_3-H_2O experiments.

Ammonia concentration, x_{NH_3}	33.5 wt%
Shell side mass flow, $\dot{m}_s$	5 - 17.5 kg/h
Shell side inlet temperature, $T_{s,in}$	50 °C
Tube side inlet temperature, $T_{t,in}$	130 °C

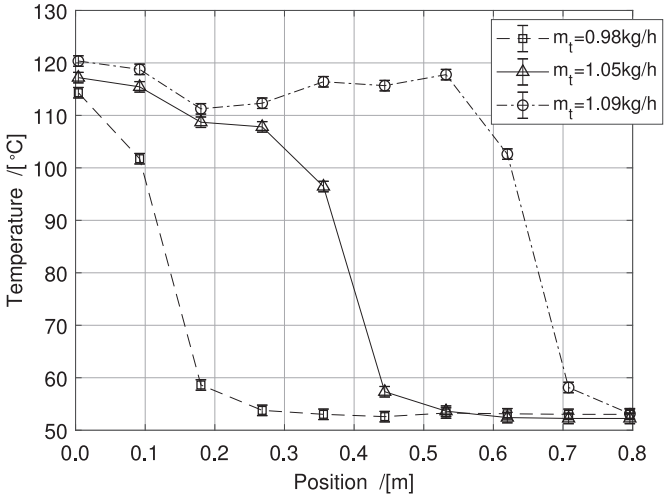

Fig. 10. Temperature results from the sensors located along the shell side of the mini-channel heat exchanger when the shell side mass flow is fixed at 7.5 kg/h for the NH_3-H_2O experiments. Error bars are included (see Section 2.2 for details). The lines serve as visual guidelines for the reader.

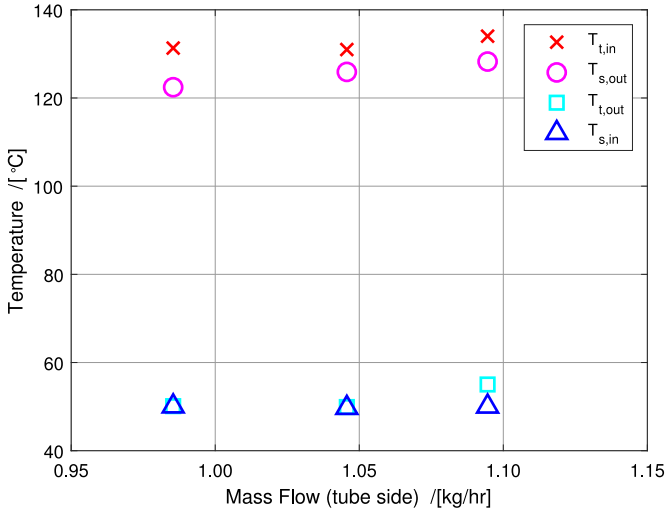

Fig. 11. In- and outlet temperatures for the NH_3-H_2O experiments at various tube side mass flows when the shell side mass flow is kept constant at 7.5 kg/h.

the tube side mass flow is around 1.05 kg/h.The results for each shell side mass flow follow a linear trend as shown in Fig. 12 and can be described with the following equation:

$$\dot{m}_t = 0.1467 \cdot \dot{m}_s \qquad for\ 5.0 \leq \dot{m}_s \leq 17.5 kg/h \tag{23}$$

Fig. 13 shows the overall heat transfer coefficient for the experiments where the maximum tube side mass flow was reached. The maximum of 6 kW/(m^{2}K) is significantly higher than the 2 kW/(m^{2}K) reported by van de Bor [18] who investigated absorption on the shell side with the same heat exchanger. This confirms that it is beneficial for the absorption process to have the NH_3-H_2O mixture on the tube side and the water on the shell side of the mini-channel. The overall heat transfer coefficient increases with increased shell side mass flow except at mass flows of 12.5 kg/h. This indicates that the tube side mass flow has not been properly optimized at this shell side mass flow. Even though the heat load is higher (see Fig. 14) the LMTD was higher than in the other cases. In this case the LMTD was higher than 3 K while in all others it was less than 2 K. In the previous experiments by van de Bor [18] the temperature sensors along the shell of the mini-channel were not installed yet. As mentioned above, they

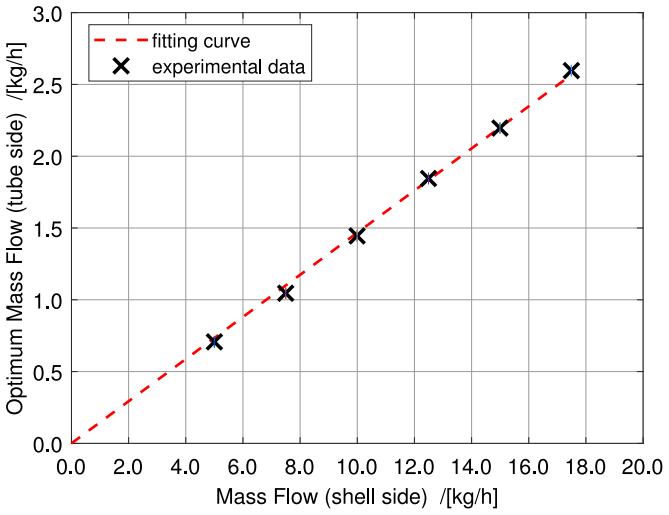

Fig. 12. The optimum tube side mass flow for each shell side mass flow of the NH_3-H_2O experiments. A clear linear trend can be seen.

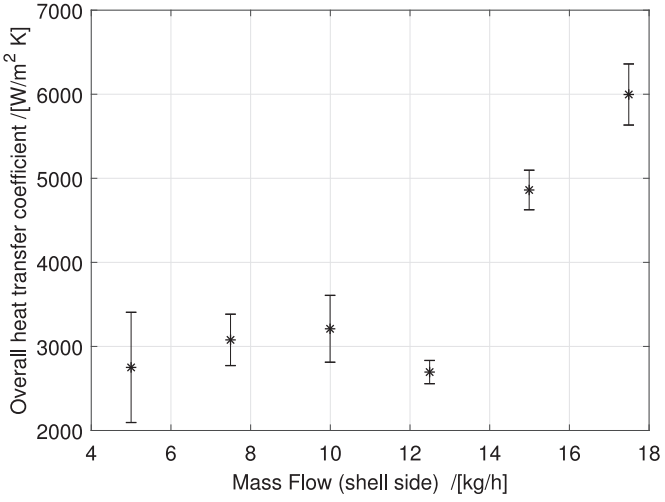

Fig. 13. The experimental overall heat transfer coefficient for the optimum tube side mass flows of the NH_3-H_2O experiments.

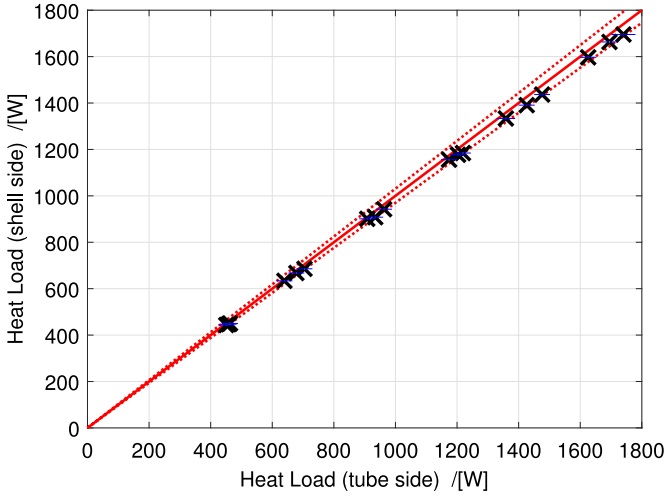

Fig. 14. The heat load on the shell and tube sides for the NH_3-H_2O experiments. The difference is within 3% (dotted line) for all the experiments.

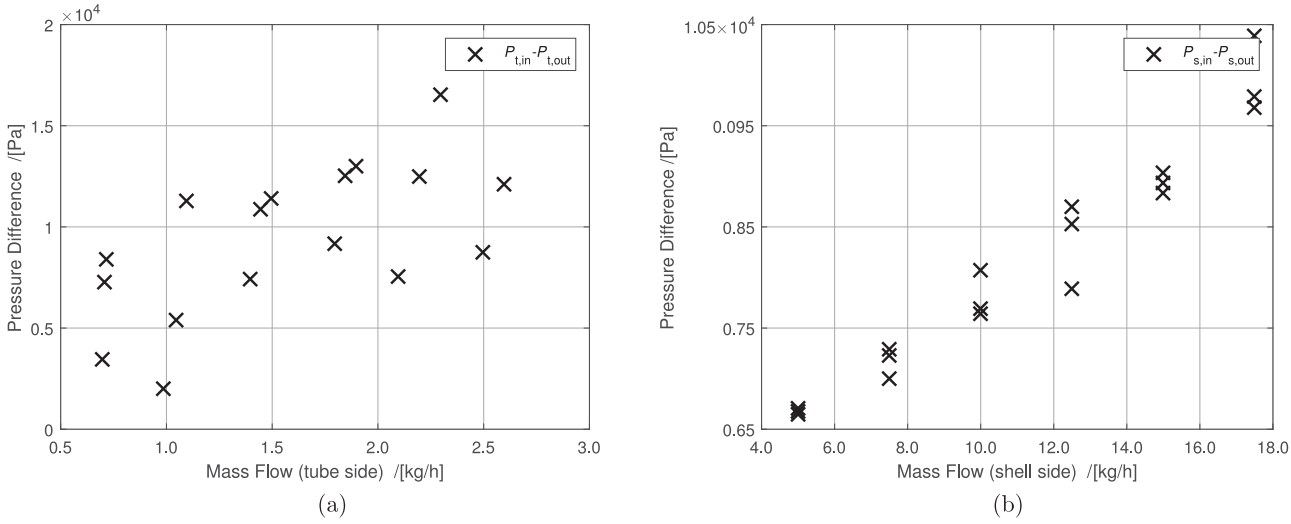

Fig. 15. Pressure drop over the mini-channel heat exchanger on the tube side (NH_3-H_2O side) (a), and the shell side (water side) (b).

show that only a limited section of the heat exchanger is used for the absorption process. With more powerful pumps it is, therefore, a possibility that even higher overall heat transfer coefficients can be reached. Fig. 14 shows the heat load on the shell and tube sides. For the NH_3-H_2O experiments the heat load of the shell side is always slightly lower than the tube side as expected because of losses to the environment. The difference is small, or always within 3%, with an average of 2.1%. The phenomenon noticed during the water-water experiments is not noticeable at all, where at higher mass flows the shell side heat load became larger than the tube side. That trend was, however, only detected at higher mass flows, above 10 kg/h. In the case of NH_3-H_2O the optimum mass flow does not exceed 3 kg/h.

The pressure drop over the shell and tube sides of the heat exchanger are shown in Fig. 15. Both of them show a trend of increased pressure drop as a function of the mass flow as expected. The trend is quite linear for both cases, although, the pressure drop on the tube side is more scattered. Since the absorption process is on the tube side it can happen that unabsorbed gas passes the heat exchanger at some point. This will affect the pressure drop over the heat exchanger which could be the reason for the scattered results.

3.3. NH_3-CO_2-H_2O experiments

After the NH_3-H_2O experiments a small amount of CO_2 was added to the tube side: 2.1 wt% CO_2. The desired testing conditions are listed in Table 5. The inlet shell and tube temperatures are kept the same as in the NH_3-H_2O experiments. The goal was to test the same range of shell side mass flows as in those experiments as well. Unfortunately, for tube side mass flows higher than 4.5 kg/h the conditions became too unstable to reach any kind of steady state. Large fluctuations in the density measured at the pump at random time intervals were observed. This indicates that unabsorbed CO_2 was still in gas phase as it passed the pump.

Table 5
Conditions to be tested during NH_3-CO_2-H_2O experiments.

Ammonia concentration, x_{NH_3}	32.8 wt%
CO_2 concentration, x_{CO_2}	2.1 wt%
Shell side mass flow, $\dot{m}_s$	5 - 17.5 kg/h
Shell side inlet temperature, $T_{s,in}$	50 °C
Tube side inlet temperature, $T_{t,in}$	130 °C

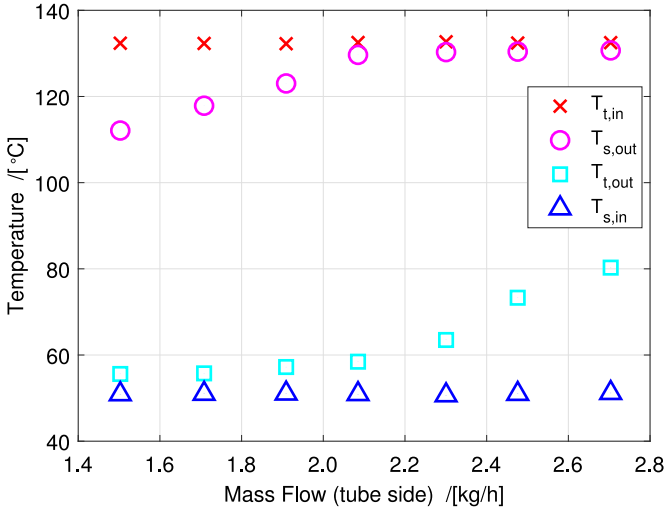

Fig. 16. The in- and outlet temperatures for the NH_3-CO_2-H_2O experiments at various tube side mass flows when the shell side mass flow is kept constant at 5 kg/h.

Therefore, it was only possible to get results for shell side mass flows of 5, 7.5 and 10 kg/h. Even though the data is limited, it can give a good indication of the influence of the added CO_2.

For the shell side mass flows of 5, 7.5 and 10 kg/h an attempt was made to find the optimum tube side mass flow with the same method as before. The temperature results for a shell side mass flow of 5 kg/h are shown in Fig. 16. For this case the optimum tube side mass flow is at around 2.1 kg/h. For each optimum tube side mass flow the temperature values at the in- and outlet are listed in Table 6. The optimum mass flow in this case can be described with the following equation:

$$\dot{m}_t = 0.43 \cdot \dot{m}_s \qquad for\ 5.0 \leq \dot{m}_s \leq 10.0 kg/h \tag{24}$$

The pressure drop results at the tube and shell sides are shown in Fig. 17. When compared to Fig. 15, it can be observed that the pressure drop at the shell side is comparable for similar mass flows. This is expected since in both cases water is at the shell side of the heat exchanger. For the mixture side, or the tube side, the pressure drop is slightly lower with the added CO_2 for similar mass flows. It should be noted that for similar mass flows the NH_3-H_2O mixture goes from being slightly superheated to subcooled. In the case of the NH_3-CO_2-H_2O mixture the mixture

Table 6
Temperature and overall heat transfer coefficient results for various shell side mass flows, with and without added CO_2 before extraction. The uncertainty of the results is obtained according to Section 2.

Parameter	Without CO_2/with CO_2	Without CO_2/with CO_2	Without CO_2/with CO_2
$\dot{m}_s$ [kg/h]	**5.00** ± 0.04/**5.00** ± 0.04	**7.50** ± 0.04/**7.50** ± 0.04	**10.00** ± 0.04/**10.00** ± 0.04
$T_{t,in}$ [°C]	**132.00** ± 0.05/**132.46** ± 0.05	**130.99** ± 0.05/**131.36** ± 0.05	**135.35** ± 0.05/**134.30** ± 0.05
$T_{s,out}$ [°C]	**127.11** ± 0.05/**131.31** ± 0.05	**125.92** ± 0.05 /**130.08** ± 0.05	**127.24** ± 0.05/**133.42** ± 0.05
$T_{t,out}$ [°C]	**50.69** ± 0.05/**58.51** ± 0.05	**49.94** ± 0.05/**58.43** ± 0.05	**50.24** ± 0.05/**54.75** ± 0.05
$T_{s,in}$ [°C]	**50.63** ± 0.05/**50.82** ± 0.05	**49.72** ± 0.05/**50.10** ± 0.05	**50.11** ± 0.05/**50.21** ± 0.05
LMTD [K]	**1.1** ± 0.3/**3.45** ± 0.05	**1.5** ± 0.1/**3.77** ± 0.08	**1.9** ± 0.2/**2.24** ± 0.07
U [kW/(m^{2}K)]	**2.7** ± 0.7/**0.94** ± 0.02	**3.1** ± 0.3/**1.280** ± 0.03	**3.2** ± 0.4 /**3.0** ± 0.1

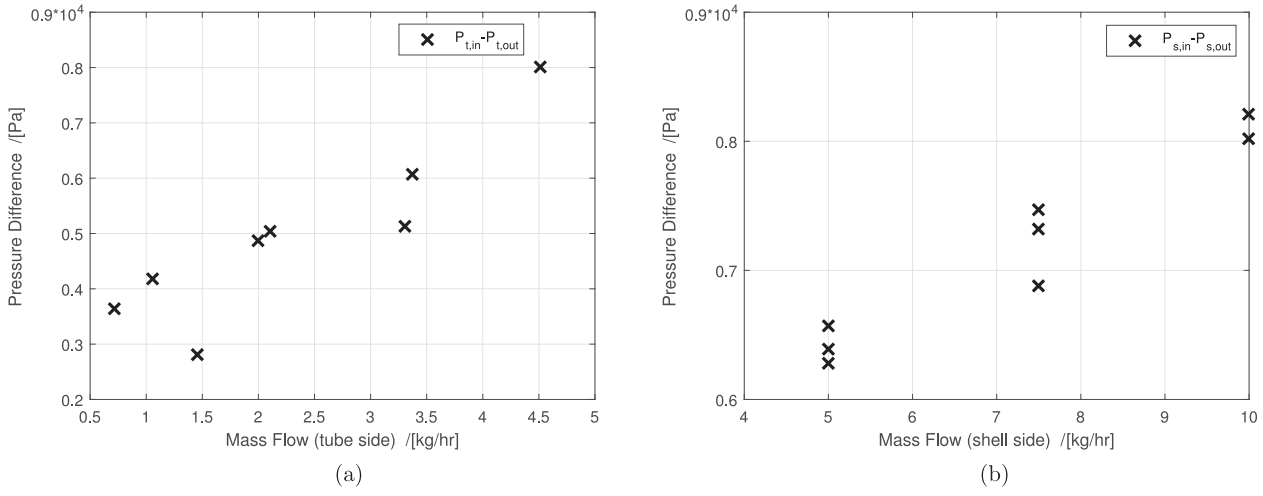

Fig. 17. Pressure drop over the mini-channel heat exchanger on the tube side (NH_3-CO_2-H_2O side) (a), and the shell side (water side) (b).

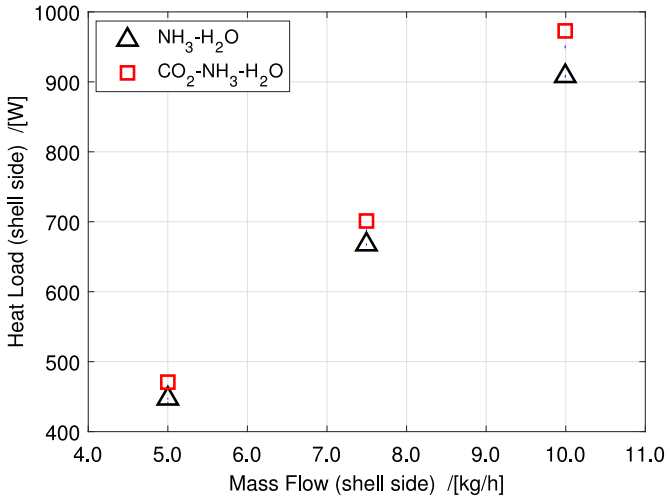

Fig. 18. Shell side heat load for the NH_3-H_2O and NH_3-CO_2-H_2O experiments.

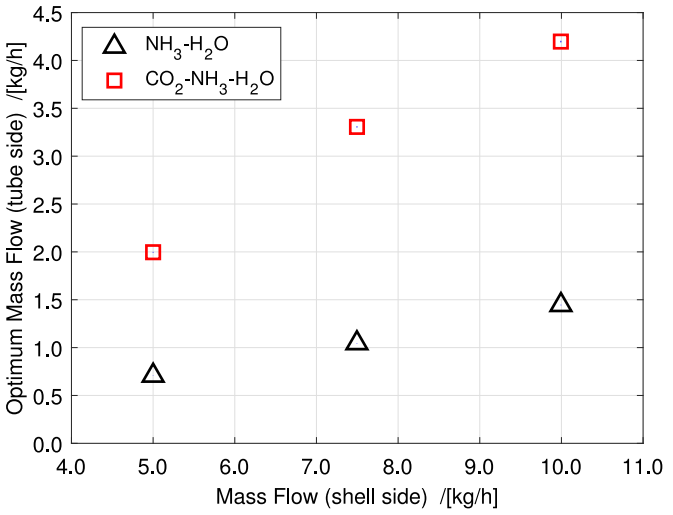

Fig. 19. Optimum tube side mass flow for the NH_3-H_2O and NH_3-CO_2-H_2O experiments for shell side mass flows of 5, 7.5 and 10 kg/h.

enters in the two-phase region and leaves the heat exchanger subcooled with associated decrease in the average velocity, which can explain the pressure drop difference.

With the added CO_2 it can be seen from Table 6 that the LMTD as well as the overall heat transfer coefficient become unfavorable. On the other hand it was noticed that the heat load increased compared to the NH_3-H_2O experiments as is clear from the shell side temperature results. The heat load for each shell side mass flow is shown in Fig. 18. The increase is around 5% for each case. These are positive results since the main goal of a heat pump is to provide heat to a heat sink. However, the optimum tube side mass flow is significantly higher with the added CO_2 (see Fig. 19). This will have a negative impact on the overall performance of CRHPs since larger mass flow means a larger power input is needed. However, with the added CO_2 the pressure increased significantly (see Fig. 20). This increase in pressure resulted in the inlet being in the two phase region. To make a fairer comparison between the two mixtures similar pressure levels are desired. Since the system is a closed loop, a part of the mixture needs to be drained to lower the pressure. To reach homogeneous conditions the system was kept at atmospheric conditions and the mixture was kept flowing to keep the same concentration after the draining process. However, when keeping the system at lower temperature the final

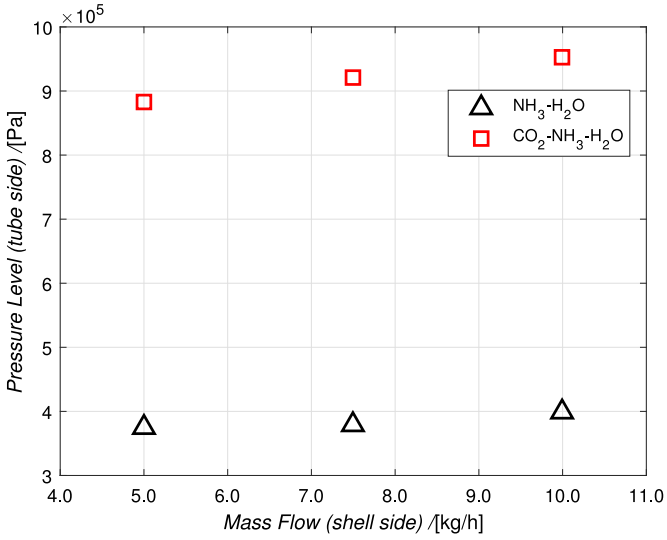

Fig. 20. Pressure levels for the NH_3-H_2O and NH_3-CO_2-H_2O experiments for shell side mass flows of 5, 7.5 and 10 kg/h.

pressure is unknown. Therefore, a couple of iterations might be needed to reach similar pressure levels.

The pressure level and shell side heat load results before and after extraction are shown in Fig. 21. The pressure during the NH_3-H_2O experiments was slightly lower than $4 \cdot 10^5$ Pa compared to around 8 - 9 $\cdot 10^5$ Pa for the first NH_3-CO_2-H_2O experiments. After the first extraction the pressure decreased slightly and the optimum tube side mass flow did indeed decrease, from around 2.1 kg/h to around 1.7 kg/h for a fixed shell side mass flow of 5 kg/h. After the second extraction the results became even better, the pressure level was still too high or around $6 \cdot 10^5$ Pa, but the optimum tube side mass flow decreased to around 1.4 kg/h. Unfortunately, after the third extraction the operation became too unstable and no steady state was reached. One plausible cause, as mentioned before, is that part of the CO_2 is unabsorbed. This also shows that the optimum mass flow is highly dependent on the operating pressure. Fig. 22 shows the temperature measured along the shell of the heat exchanger for the NH_3-CO_2-H_2O and NH_3-H_2O at shell side mass flows of 5 kg/h. From the figure it can be seen that the absorption process takes up a significantly larger section of the mini-channel for the NH_3-CO_2-H_2O mixture compared to the NH_3-H_2O mixture. The figure also shows clearly that larger mass flows are needed to reach comparable or better performance with the added CO_2 for these specific operating conditions.

3.4. Experimental challenges for upward and downward flow direction in the tube

The randomness of the spikes in the mass flow after the last extraction pointed to a pocket of CO_2 gas building up somewhere in the system. Likely at the top of the heat exchanger. To further investigate this, experiments were performed where the absorption process is from the bottom to the top of the mini-channel heat exchanger instead of top to bottom. As reported by Bhagwat and Ghajar [32] the flow patterns and void fractions differ quite significantly between vertical two phase downward and upward flow. For the third extraction where no steady state was reached at all when the absorption process was from top to bottom, it was now easily reached for the bottom to top absorption configuration. Fig. 23 shows the temperatures measured along the shell side of the heat exchanger for absorption in both upward and downward flow. From the figure it is clear that the trend differs significantly between the two absorption operating modes. The mass flows and the heat duties are listed in Table 7 and compared to the results from the downward flow without extraction and from the NH_3-H_2O experiments. The optimum tube side mass flow decreased, however, the heat transfer became worse by approximately 10%. This is contradictory to the findings of Kang et al. [9] and Castro et al. [10] where bubble absorption was more favorable than falling film absorption. This difference indicates that the geometry plays a large role in the absorption process and it is likely that for other compact heat exchangers the findings would be similar as in this case.

This also indicates that the configuration of the heat exchanger becomes very important when operating with an NH_3-CO_2-H_2O mixture. Other heat exchangers might be better suited for NH_3-CO_2-H_2O than the mini-channel heat exchanger used for the experiments. It is unlikely that plate heat exchangers are well suited since the mixture passed through a plate heat exchanger before the pump in the setup. In the plate heat exchanger the mixture is subcooled by more than 30 K. Still, the CO_2 was not

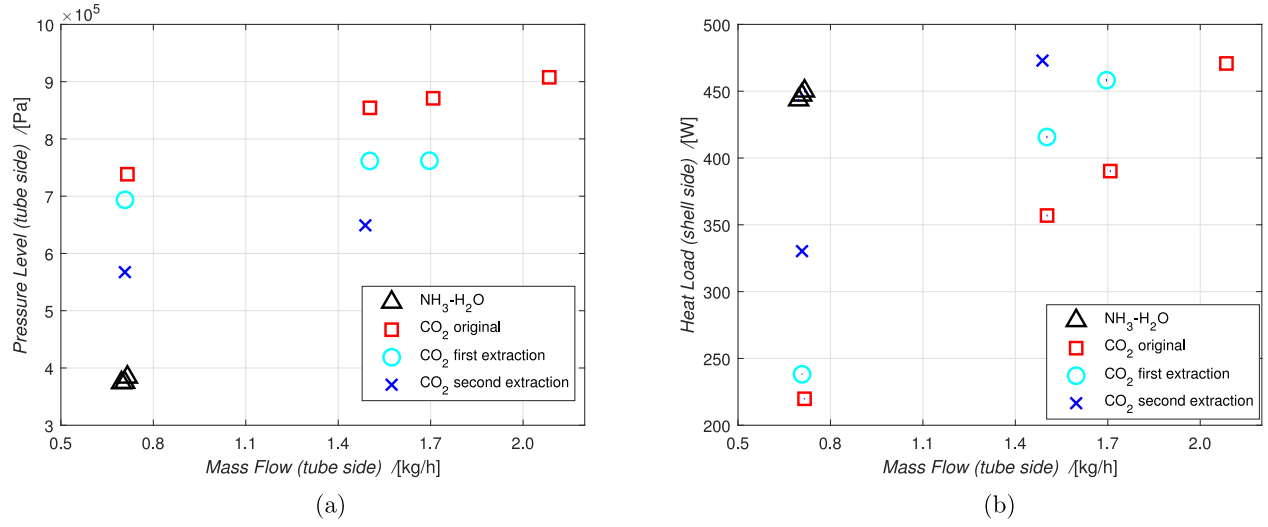

Fig. 21. Results for a shell side mass flow of 5 kg/h before and after draining of the mixture with added CO_2 compared to the NH_3-H_2O results, the different pressure levels (a), and the shell side heat load (b). It is clear that comparable pressure levels were not reached with the added CO_2. However, with each extraction the performance at similar mass flows approached the performance of the NH_3-H_2O mixture.

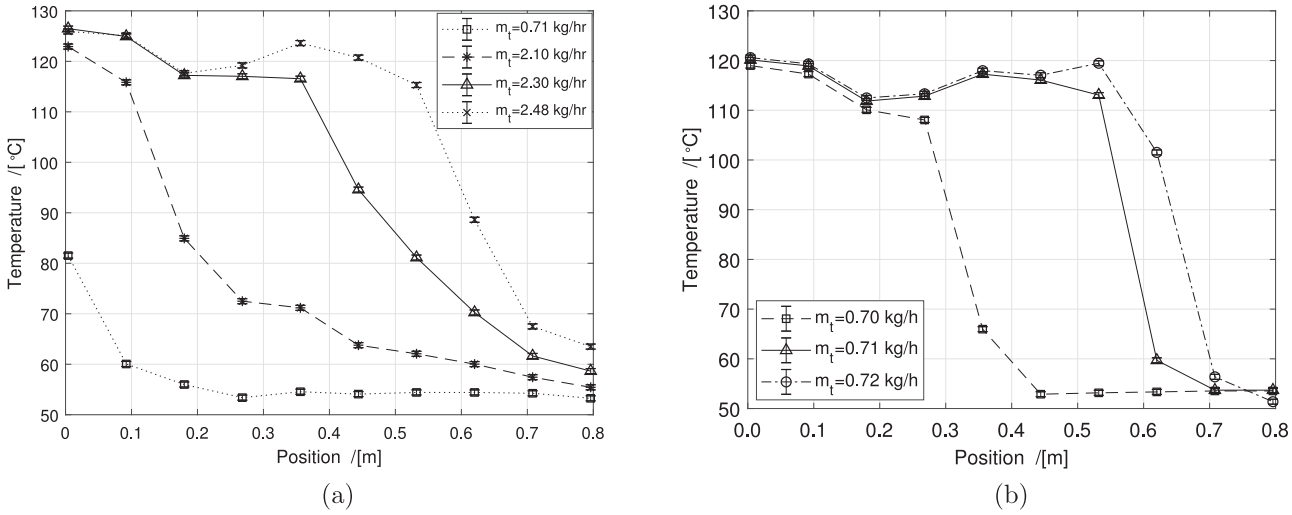

Fig. 22. Temperature results from the sensors located along the shell side of the mini-channel heat exchanger for a shell side mass flow of 5 kg/h, for the NH_3-CO_2-H_2O mixture (a), and the NH_3-H_2O mixture (b). Error bars are included (see Section 2 for details). The lines serve as visual guidelines for the reader.

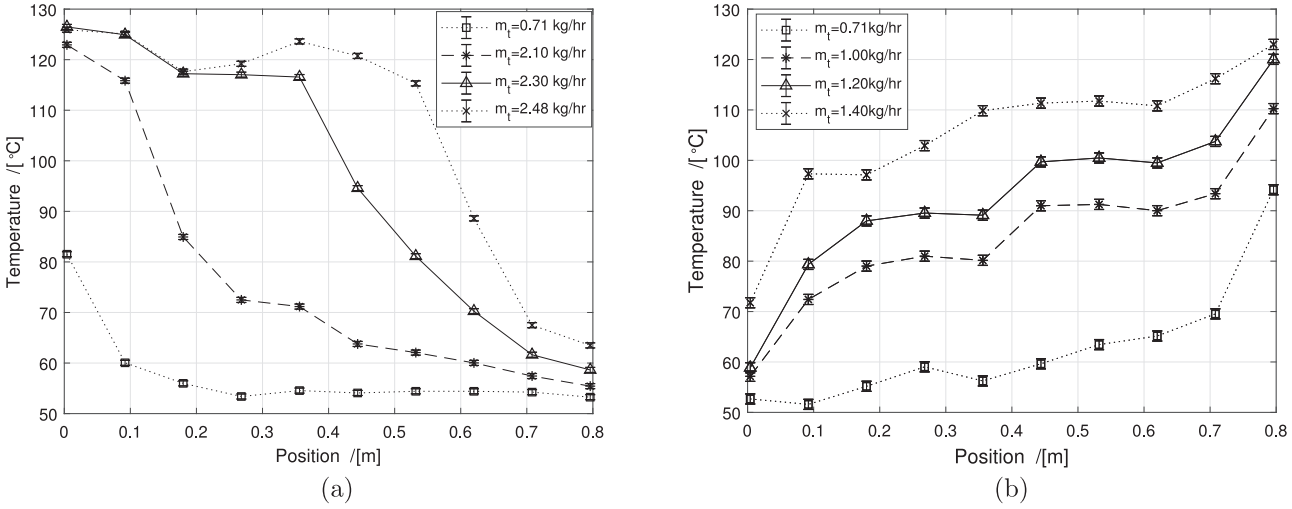

Fig. 23. Temperature results from the sensors located along the shell side of the mini-channel heat exchanger for a shell side mass flow of 5 kg/h, for absorption in downward flow of the NH_3-CO_2-H_2O mixture (a), and in upward flow of the NH_3-CO_2-H_2O mixture (b). Error bars are included (see Section 2 for details). The lines serve as visual guidelines for the reader.

Table 7
Comparison of the tube side optimum mass flow and uncertainty-weighted average heat load when operating at different shell side mass flows for NH_3-H_2O, NH_3-CO_2-H_2O absorption in downward flow and NH_3-CO_2-H_2O absorption in upward flow.

Mixture	$\dot{m}_s$ [kg/h]	$\dot{m}_{t,opt}$ [kg/h]	$\bar{Q}$ [W]
NH_3-H_2O (downward flow)	**5.00** ± 0.04	**0.71** ± 0.04	**447** ± 4
	7.50 ± 0.04	**1.05** ± 0.04	**668** ± 4
	10.00 ± 0.04	**1.40** ± 0.04	**901** ± 4
NH_3-CO_2-H_2O (downward flow)	**5.00** ± 0.04	**2.10** ± 0.04	**462** ± 1
	7.50 ± 0.04	**3.30** ± 0.04	**693** ± 2
	10.00 ± 0.04	**4.20** ± 0.04	**970** ± 2
NH_3-CO_2-H_2O (upward flow)	**5.00** ± 0.04	**1.20** ± 0.04	**418** ± 1
	7.50 ± 0.04	**1.80** ± 0.04	**615** ± 1
	10.00 ± 0.04	**2.40** ± 0.04	**888** ± 2

fully absorbed at certain conditions. The experiments with absorption in upward flow resulted in increased stability. Therefore, it might be sufficient to redesign the top part of the heat exchanger in such a way that accumulation of gaseous CO_2 would be eliminated or limited. Another solution would be to increase the absorption rate. Different measures have been proposed to achieve this. As mentioned in the introduction, it has been shown experimentally that smaller diameters increase the absorption rate [11,14]. Therefore, it could be beneficial to use a micro-channel heat exchanger with even smaller channels, since this might be sufficient to get rid of gas pockets of CO_2. Another way could be to increase the surface roughness of the tubes, both Kim et al. [33] and Park et al. [28] showed that the absorption performance increased significantly by only increasing the surface roughness.

Another important factor to take into account is that in CRHPs there is no pump. The unabsorbed CO_2 might still be a problem for the expansion device after the absorber, however, for the rest of the components, the desorber and the compressor, it isn't.

3.5. Material compatibility with added CO_2

The components in the experimental setup have been carefully chosen to be compatible with NH_3-H_2O. Most components are stainless steel. With the added CO_2 it is a question if the setup is still compatible. One of the dangers of adding CO_2 to NH_3-H_2O is the chance of solid formation, mainly of ammonium bicarbonate. Therefore, before initiating the experiments the properties of the NH_3-CO_2-H_2O mixture were investigated by Gudjonsdottir et al. [3]. They developed a new fit of the existing e-NRTL (electrolyte - Non-Random Two-Liquid) method available in the Aspen Plus software [34] suitable for the range that is interesting for CRHP applications. With only 2.1 wt% of CO_2, when the NH_3 concentration is above 30 wt%, there is no danger of solid formation at room temperatures. Much higher concentration of CO_2 is needed or around 20 wt%. With the same method the pH level of the mixture can be investigated. CO_2 in water results in an acid solution, however, NH_3 in water results in a basic solution. The mixture concentration used in the experiments has much higher concentration of NH_3 than CO_2 and, therefore, the mixture is basic. For the temperature range that is investigated the pH level is in the range of 8 - 10. After conduction the experiments the setup has been partly taken apart and no corrosion or solid formation of any kind was visible.

4. Conclusions

In this paper experiments were performed in a mini-channel heat exchanger to verify the benefits of utilizing NH_3-CO_2-H_2O, rather than NH_3-H_2O, for heat pump applications. Additional goal was to verify which configuration achieves higher absorption performance. That is if the mixture should be on the tube or shell side and if absorption in downward or upward flow should be used. The main conclusions are the following:

- For increased performance the mixture should be on the tube side of the mini-channel heat exchanger. Overall heat transfer coefficients of 6 kW/(m^2K) were reached compared to only 2 kW/(m^2K) when the mixture was kept on the shell side [18].
- Absorption in downward flow is preferred. With the present heat exchanger design, the performance increased by approximately 10% compared to absorption in upward flow.
- The mixture mass flow that results in better results in terms of temperature difference and overall heat transfer coefficient is highly dependent on the operating pressure.
- A heat load increase of approximately 5% was observed for the NH_3-CO_2-H_2O mixture compared to NH_3-H_2O. However, pumping instabilities limited the operating range. Therefore, these results are based on limited data and comparable pressure ranges were not accomplished.

The encountered pumping instabilities indicate that specific absorbers might be necessary for optimum performance when operating with NH_3-CO_2-H_2O, such as micro-channel heat exchangers or a mini-channel heat exchanger with a specially designed inlet that minimizes the risk of accumulation of CO_2. It is, therefore, recommended to study the performance of NH_3-CO_2-H_2O in microchannel heat exchangers and over a larger operating range. Further, it is recommended to further study the compressor performance with added CO_2 and the performance when implemented in an entire heat pump cycle.

Declaration of Competing Interest

There is no conflicts of interests.

CRediT authorship contribution statement

V. Gudjonsdottir: Conceptualization, Methodology, Formal analysis, Investigation, Data curation, Writing - original draft. **L. Shi:** Data curation, Formal analysis, Writing - review & editing. **C.A. Infante Ferreira:** Supervision, Writing - review & editing, Funding acquisition, Project administration, Resources, Conceptualization.

Acknowledgments

The authors would like to thank the members of the ISPT "Upgrading waste streams with compression resorption heat pumps" project for their financial and in kind contributions. This project was supported by the following organizations: ISPT, TU Delft, DOW, Nouryon, Atlas Copco, IBK, Frames. This project received funding from TKI E&I with the supplementary grant 'TKI-Toeslag' for Top-consortia for Knowledge and Innovation (TKI's) of the Ministry of Economic Affairs and Climate Policy.

References

[1] UNCC, The Paris Agreement, 2016, Https://unfccc.int/process/the-paris-agreement/what-is-the-paris-agreement.
[2] IEA, Application of industrial heat pumps, 2014, Technical report. https://www.energiteknologi.dk/sites/energiteknologi.dk/files/slutrapporter/annex_xiii_part_a.pdf.
[3] V. Gudjonsdottir, C.A. Infante Ferreira, G. Rexwinkel, A.A. Kiss, Enhanced performance of wet compression-resorption heat pumps by using NH_3-CO_2-H_2O as working fluid, Energy 124 (2017) 531—542.
[4] N.A.A. Qasem, S.M. Zubair, Compact and microchannel heat exchangers: acomprehensive review of airside friction factor and heat transfer correlations, Energy Convers. Manage. 173 (2018) 555—601.
[5] M.G. Khan, A. Fartaj, A review on microchannel heat exchangers and potential applications, Int. J. Energy Res. 35 (2011) 553—582.
[6] C. Amaris, M. Vallès, M. Bourouis, Vapour absorption enhancement using passive techniques for absorption cooling/heating technologies: a review, Appl. Energy 231 (2018) 826—853.
[7] D. Trichè, S. Bonnet, M. Perier-Muzet, F. Boudèhenn, H. Demasles, N. Caney, Experimental and numerical study of a falling film absorber in an ammonia-water absorption chiller, Int. J. Heat Mass Transf 111 (2017) 374—385.
[8] A.K. Nagavarapu, S. Garimella, Experimentally validated models for falling-film absorption around microchannel tube banks: hydrodynamics, Int. J. Heat Mass Transf. 134 (2019) 815—827.
[9] Y.T. Kang, A. Akisawa, T. Kashiwagi, Analytical investigation of two different absorption modes: falling film and bubble types, Int. J. Refrig. 23 (2000) 430—443.
[10] J. Castro, C. Oliet, I. Rodríguez, A. Oliva, Comparison of the performance of falling film and bubble absorbers for air-cooled absorption systems, Int. J. Therm. Sci. 48 (2009) 1355—1366.
[11] J. van Leeuwen, Absorption and desorption of ammonia-water mixtures in mini-channel heat exchangers, 2011, Master thesis, Delft University of Technology.
[12] S. Garimella, M.D. Determan, J.M. Meacham, S. Lee, T.C. Ernst, Microchannel component technology for system-wide application in ammonia/water absorption heat pumps, Int. J. Refrig. 34 (2011) 1184—1196.
[13] D.M. van de Bor, C. Vasilescu, C.A. Infante Ferreira, Experimental investigation of heat transfer and pressure drop characteristics of ammoniaâ-water in a mini-channel annulus, Exp. Therm Fluid Sci. 61 (2015) 177—186.
[14] C. Amaris, M. Bourouis, M. Vallès, Effect of advanced surfaces on the ammonia absorption process with NH_3/$LiNO_3$ in a tubular bubble absorber, Int J. Heat Mass Transf. 72 (2014) 544—552.
[15] J.I. Yoon, T.T. Phan, C.G. Moon, H.S. Lee, S.K. Jeong, Heat and mass transfer characteristics of a horizontal tube falling film absorber with small diameter tubes, Heat Mass Transf. 44 (2008) 437—444.
[16] P. Stephan, S. Kabelac, M. Kind, H. Marting, D. Mewes, K. Schaber, VDI Heat Atlas, second, Springer, Berlin, 2010.
[17] C.W.M. Nefs, D. van de Bor, C.A. Infante Ferreira, Laminar single phase flow distribution in a multi-tube mini-channel heat exchanger using fractal distribution, Chem. Eng. Process. 80 (2014) 29—37.
[18] D. van de Bor, Mini-channel heat exchangers for industrial distillation processes, 2014, PhD thesis, Delft University of Technology, https://repository.tudelft.nl/islandora/object/uuid%3A737def3e-897a-4153-8f57-791a8afa14a8?collection=research.
[19] K.B. Lee, B.H. Chun, G.C. Lee, S.H. Kim, Experimental analysis of bubble mode in a plate-type absorber, Chem. Eng. Sci. 57 (2002) 1923—1929.

[20] S. Lee, L.K. Bohra, S. Garimella, A.K. Nagavarapu, Measurement of absorption rates in horizontal-tube falling-film ammonia-water absorbers, Int. J. Refrig. 35 (2012) 613—632.
[21] J. Cerezo, R. Best, M. Bourouis, A. Coronas, Comparison of numerical and experimental performance criteria of an ammonia-water bubble absorber using plate heat exchangers, Int. J. Heat Mass Transf. 53 (2010) 3379—3386.
[22] Y.T. Kang, A. Akisawa, T. Kashiwagi, Experimental correlation of combined heat and mass transfer for NH_3-H_2O falling film absorption, Int. J. Refrig. 22 (1999) 250—262.
[23] C. Ozgur, Demonstration plant design: Two conventional distillation columns integrated with two novel heat pumps, 2012, PDEng report, Delft University of Technology.
[24] M.J. Moran, H.N. Shapiro, Fundamentals of Engineering Thermodynamics, John Wiley and Sons, 6th edition, 2010.
[25] E.W. Lemmon, M.L. Huber, M.O. McLinden, 2013, NIST Standard Reference Database 23: Reference Fluid Thermodynamic and Transport Properties-REFPROP, Version 9.1, National Institute of Standards and Technology, Standard Reference Data Program, Gaithersburg.
[26] Y.G. Park, L. Liu, A.M. Jacobi, Rational approaches for combining redundant, independent measurements to minimize combined experimental uncertainty, Exp. Therm. Fluid Sci. 34 (2010) 720—724.
[27] J. Taylor, Introduction to Error Analysis, the Study of Uncertainties in Physical Measurements, University Science Books, US, 1997.
[28] C.W. Park, S.S. Kim, H.C. Cho, Y.T. Kang, Experimental correlation of falling film absorption heat transfer on micro-scale hatched tubes, Int. J. Refrig. 26 (2003) 758—763.
[29] E.M. Sparrow, S.V. Patankar, Relationships among boundary conditions and Nusselt numbers for thermally developed duct flows, J. Heat Transf. 99 (1977) 483—484.
[30] O. Miyatake, H. Iwashita, Laminar-flow heat transfer to a fluid flowing axially between cylinders with a uniform wall heat flux, Int. J. Heat Mass Transf. 34 (1991) 322—327.
[31] D.M. van de Bor, C.A. Infante Ferreira, A.A. Kiss, Optimal performance of compression-resorption heat pump systems, Appl. Therm. Eng. 65 (2014) 219—225.
[32] S.M. Bhagwat, A.J. Ghajar, Similarities and differences in the flow patterns and void fraction in vertical upward and downward two phase flow, Exp. Therm. Fluid Sci. 39 (2012) 213—227.
[33] J.K. Kim, C.W. Park, Y.T. Kang, The effect of micro-scale surface treatment on heat and mass transfer performance for a falling film h_2o/libr absorber, Int. J. Refrig 26 (2003) 575–585.
[34] Aspen Physical Property System, Version 8.8, 2015, Aspen Tech, Cambridge, MA.